Realistic Model of Charge Mobility in π-conjugated Polymer Systems

Laszlo Berencei,[1,2,a)] Alice Grout-Smith,[1,3] Jessica Ellen Poole,[1,2] and William Barford[1,2,b)]

[1)] *Department of Chemistry, Physical and Theoretical Chemistry Laboratory, University of Oxford, Oxford, OX1 3QZ, United Kingdom*

[2)] *Balliol College, University of Oxford, Oxford, OX1 3BJ, United Kingdom*

[3)] *Hertford College, University of Oxford, Oxford, OX1 3BW, United Kingdom*

Charge transfer processes and charge mobility are investigated in the poly(p-phenylenevinylene) (PPV) model system. Realistic disordered polymer conformations are created and used in a coarse-grained model. Localized and quasi-extended states are obtained using the Holstein Hamiltonian. Charge transport is modeled as an incoherent hopping mechanism in the framework of unimolecular and bimolecular Marcus theory for intramolecular and intermolecular processes, respectively, to account for the electron-phonon coupling present in π-conjugated polymer systems. Static and quasi-dynamic disorder effects are both considered using the 'fluctuating bridges' approach. Charge mobility is calculated using kinetic Monte Carlo simulations for a range of physically relevant parameters. We examine the relative importance of intramolecular and intermolecular mechanisms, and the role of localized and extended states in the transport process. We discuss the role of disorder and temperature, and show that a $\log \mu \propto -\sqrt{F}$ electric field dependence in the high field regime naturally emerges from our model. We show that disorder significantly reduces the mobility at low fields, but slightly increases it at high fields. We also show that the mobility is dominated by inter-chain charge transfer between low energy localized states at low fields, but at higher fields intra-chain transfer to more delocalized higher energy states becomes equally important. This cross-over is the cause of anisotropic charge mobility at intermediate field strengths.

[a)] Electronic mail: laszlo.berencei@chem.ox.ac.uk

[b)] Electronic mail: william.barford@chem.ox.ac.uk

I. INTRODUCTION

Conjugated organic semiconductors, such as poly(p-phenylenevinylene) (PPV) have been of great interest to the research community for their potential application in electronic devices such as organic light-emitting diode (OLED) displays, field-effect transistors and photovoltaic devices.[1–3] Their favorable structural properties and ease of manufacturing mean they can be considered as an alternative class of materials to the currently widely used inorganic, silicon-based ones.[4,5] The major limiting factor to their applicability is their significantly lower charge mobility compared to their inorganic counterparts. In this work, a novel, atomistic model is developed to understand the mechanism of charge mobility in bulk PPV systems.

Charge mobility in conjugated polymer films is affected by a number of intrinsic properties, such as disorder, polaronic effects and chain conformation. Previous theoretical work in the field established that charge transfer in conjugated polymer systems is an incoherent hopping process. In particular, Bässler's influential work[6] models the electronic states as a set of Anderson localized states due to disorder. Linked to the absorption line shapes of such systems, these states are modeled to follow a Gaussian shaped distribution of energies, giving rise to the Gaussian Disorder Model (GDM). This ansatz, and improved model systems incorporating spatially correlated disorder,[7–9] while not soluble analytically, through numerical simulations provide a good theoretical description of model disorder in conjugated polymer systems.

Within the GDM, the charge mobility, μ, at sufficiently low electric fields, F, is understood[6–11] to be governed by disorder and temperature as

$$\mu = \mu_0 \exp\left[-\left(\frac{E_a}{k_B T}\right)\right] \exp\left[-C_1 \left(\frac{\sigma}{k_B T}\right)^2\right] \times \exp\left[C_2 \left\{\left(\frac{\sigma}{k_B T}\right)^2 - \Sigma^2\right\} \sqrt{F}\right], \tag{1}$$

where μ_0 is the zero-field charge mobility in the $T \to \infty$ limit, E_a is the polaron activation energy, σ is the width of the energetic disorder, Σ is the width of the disorder in the transfer integrals, and C_i are constants. This description confirms the validity of the Gaussian density of states model, the role of disorder and polaron effects. This is also consistent with the experimentally observed Poole-Frenkel behavior,[12] which indicates a $\log \mu \propto \sqrt{F}$

dependence over a range of electric field strength values.

In alternative approaches, the well-known formation of polarons in quasi one-dimensional system, via a Marcus theory[13] analysis, was found to lead to a reduction in the mobility at high fields, owing to the inverted Marcus regime.[14,15]

These predictions are in semi-quantitative agreement with experiment. As observed by Fornari and Troisi,[16] however, a key step is still to relate this theoretical understanding based on model systems to realistic systems, and thus to make fully quantitative predictions based on structure-property relationships. Moreover, studies of realistic systems highlight significant approximations in most theoretical models. For example, most models treat quantities such as donor-acceptor separation and polaron relaxation energies as parameters independent of the system disorder, which they are clearly not. Additionally, most models assume nearest-neighbor charge transfer, whereas longer-range transfer via quasi-extended states is also possible.[17,18] Finally, most models ignore the highly anisotropic nature of charge transfer in polymeric systems, whereas intra-chain and inter-chain charge transfer can occur at significantly different rates.[19]

The first step towards such a realistic model came from Jakobsson et al[20] who performed simulations of PV oligomer systems, modeling intermolecular charge transfer using unimolecular Marcus rate theory. However, reorganization energies were still treated parametrically, and for the chosen model parameters and field strength values they failed to reproduce the reduction in mobility at high fields, which is expected due to the inverted Marcus regime.[14,21]

The model presented in this work combines and extends a number of the ideas introduced above. Charge mobility in bulk PPV systems is simulated by building an ensemble of long, conformationally disordered polymer chain geometries, intended to explore the consequences of more realistic modeling over idealized models. Conformationally static and on-site disorder leads to classes of Anderson localized and quasi-extended donor and acceptor states.[22,23] The realistic treatment of disorder leads to an almost Gaussian distribution of states, providing a clear link to Bässler's GDM model. Inter-chain and intra-chain charge transfer are separately accounted for, using a bimolecular Marcus rate theory for the former. Intra-chain charge transfer is examined in the framework of Troisi and co-workers' unimolecular Marcus theory via 'fluctuating bridges'.[16,18] The Marcus-type transition rate expressions therefore incorporate polaronic effects through the reorganization energy terms. The inter-state hopping is not restricted to nearest-neighbor donor and acceptor states, but

allows for hopping between states at a range of spatial separations, as discussed in detail in Section III B. Since our model describes the disorder-dependent spatial extent of the donor and acceptor states, it also predicts the disorder-dependent relaxation energies that appear in the Marcus expressions. Finally, electronic overlaps are also calculated using a realistic formalism, which takes into account the effect of torsional disorder in the chain, resulting in a physical account of off-diagonal disorder.

Our results highlight the relative importance of intramolecular versus intermolecular charge transfer; the role of more localized states versus extended states as a function of field strength; and the role of disorder on determining mobility. The results from our more realistic simulations are also broadly in agreement with the low field behaviour indicated by Eq. (1).

We begin in Section II by describing the model Hamiltonians used in our simulation program, as well as introducing the coarse-graining of PPV polymer chain geometries into a reduced dimensionality problem. In Section III we define the localized and extended states arising by solving the system Hamiltonian under the influence of energetic and structural disorder. Section IV describes the charge transfer rates between these states in the framework of unimolecular and bimolecular Marcus theory. In Section V we show how realistic PPV morphologies are generated, and how a kinetic Monte Carlo simulation scheme was implemented to model charge dynamics and obtain charge mobility values. We present our results in Section VI, examining the effect of disorder, temperature and electric field on charge mobility in our system, first, in Section VI A, restricted to the localized states of the system, and then in Section VI B we explore the role of the extended states as potential acceptors. Our conclusions in Section VII compare and contrast our results with previous work in the field (both theoretical and experimental), and discuss future directions of research.

II. MODEL HAMILTONIANS

A. Hückel model

Our model describes PPV using a π-electron model, meaning that only the electrons in the delocalized π-system are considered, independently of the σ-bonding framework of the molecule. A single p_z-orbital per C-atom on the carbon framework of the molecule is

considered. The simplest such model is the Hückel model, which can be written in the atomic basis as

$$\hat{H}^{\text{atomic}}_{\text{Hückel}} = -\sum_i t_i \left(\hat{c}_i^\dagger \hat{c}_{i+1} + \hat{c}_{i+1}^\dagger \hat{c}_i \right), \tag{2}$$

where t_i is the transfer integral between nearest neighbor atomic orbitals, and $\hat{c}_i^\dagger$ and $\hat{c}_i$ correspond to the creation and destruction of an electron in orbital i, respectively. There is no term corresponding to the on-site energies of orbitals, as the p_z-orbitals are degenerate and their energies can be set to zero.

B. Coarse-graining

The degrees of freedom considered in the model are reduced by coarse-graining the polymer molecules into chains of "sites", with a site corresponding to a monomer moiety (i.e., two sites for the phenylene and vinylene moieties per monomer). This is illustrated in Fig. 1. In the coarse-grained model, the atomic basis $\{|i\rangle\}$ is replaced by the moiety basis $\{|n\rangle\}$, where n corresponds to either a phenylene or a vinylene moiety. Therefore, we now redefine our creation and destruction operators to correspond to the new coarse-grained basis

$$|i\rangle = \hat{c}_i^\dagger |0\rangle \qquad \Rightarrow \qquad |n\rangle = \hat{a}_n^\dagger |0\rangle. \tag{3}$$

The new, coarse-grained Hückel Hamiltonian is thus

$$\hat{H}^{\text{cg}}_{\text{Hückel}} = \sum_n \epsilon_n \hat{a}_n^\dagger \hat{a}_n - \sum_n \tilde{t}_n \left(\hat{a}_n^\dagger \hat{a}_{n+1} + \hat{a}_{n+1}^\dagger \hat{a}_n \right). \tag{4}$$

The first term in Eq. (4) are the on-site energies, with ϵ_n taking different values for even and odd sites, corresponding to the different moieties in PPV. The transfer (or hopping) term is defined as

$$\tilde{t}_n = \tilde{t}_0 \cos(\phi_n), \tag{5}$$

with ϕ_n denoting the dihedral angle between neighboring polymer moieties, and $\tilde{t}_0$ the transfer integral between planar moieties. The coarse-grained $\tilde{t}_0$ it linked to t_0 in the atomic basis set by $\tilde{t}_0 = t_0/\sqrt{6}$, arising as the product of orbital coefficients on the linking carbon atoms in the LUMO states of the phenylene and vinylene moieties, $1/\sqrt{2}$ and $1/\sqrt{3}$, respectively, as defined by the atomic orbital coefficients illustrated in Fig. 2.

The model Hamiltonian is solved for these coarse-grained sites, then the wavefunction amplitude is calculated for each p_z-orbital as a product of the wavefunction amplitude for

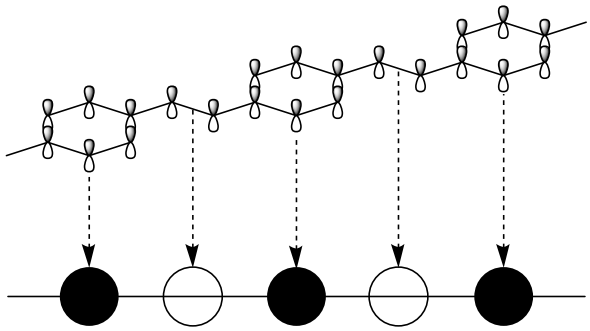

FIG. 1: The coarse-graining of PPV into two sites per monomer, corresponding to each phenylene and vinylene moiety.

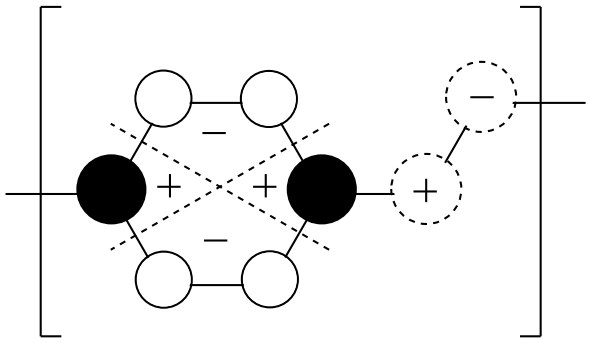

FIG. 2: Coefficients of the atomic orbitals, φ_i, contributing to the local LUMO wavefunctions of PPV. $\varphi_{\text{filled}} = 1/\sqrt{3}$, $\varphi_{\text{unfilled}} = 1/\sqrt{12}$, $\varphi_{\text{dashed}} = 1/\sqrt{2}$, with the signs of these coefficients indicated accordingly.

the corresponding site, ψ_n, from solving Eq. (4), and that of the orbital coefficient, φ_i, on a given atom in the local LUMO orbitals of the given moiety (as shown in Fig. 2).

C. Holstein model

Electron transfer occurs between the lowest unoccupied molecular orbitals (LUMO) (or equivalently, hole transfer between the highest occupied molecular orbitals, HOMOs) in each moiety. The system is described by the Holstein model,[24,25] which is a tight-binding Hamiltonian, with added terms to account for electron-phonon couplings to model polaronic effects. The Holstein model is defined as

$$\hat{H}_{\text{Holstein}} = \hat{H}^{\text{cg}}_{\text{Hückel}} - \hbar\omega \sum_n A_n \tilde{Q}_n \hat{a}^\dagger_n \hat{a}_n + \frac{\hbar\omega}{2} \sum_n \tilde{Q}^2_n, \tag{6}$$

where $\hat{H}^{\mathrm{cg}}_{\mathrm{Hückel}}$ is defined in Eq. (4). The second term accounts for electron-phonon coupling to a local vibrational mode, $\tilde{Q}_n$, with coupling strength A_n, where the Huang-Rhys parameter $S_n = A_n^2/2$. The final term denotes the elastic energy of the normal mode. The last two terms are expressed as a function of the dimensionless normal coordinates, $\tilde{Q}_n$, defined as $\tilde{Q}_n = (\mu\omega/\hbar)^{1/2} Q_n$, where μ is the reduced mass of the normal mode and ω is its angular frequency.[26] Only the coupling to a single local normal mode for each moiety is considered. The values of the parameters in the Hamiltonians are summarized in Table I.

III. DONOR AND ACCEPTOR STATES

A. Role of polaronic effects

In the adiabatic *limit*, i.e., $\hbar\omega/t \to 0$, electron-phonon coupling causes self-localized Landau polarons.[24,25] However, as shown in refs 27,28 (and noted by Fornari and Troisi[16]), in the adiabatic *regime* relevant to conjugated polymers (i.e., $\hbar\omega/t \sim 0.1$), the self-localization length scale is much larger than the localization length caused by disorder (as discussed in Section III B). Thus, the "polaronic" effects considered here are "self-trapping", i.e., a reorganization energy that appears in the Marcus rate expressions (see Section IV), but not a self-localized charge wavefunction.

B. Role of disorder

In real polymer systems fluctuations in density (and therefore in the local electrostatic environment) and torsional motion in the molecules result in fluctuations in the on-site energy terms, ϵ_n, and through fluctuations in the torsional angles, ϕ_n, in the off-diagonal transfer terms, $\tilde{t}_n$ as per Eq. (5). Such disorder results in the localization of states along the polymer chains through Anderson localization.[22,23,29] The lowest energy states will be highly localized, quasi-nodeless states, extending over a few monomers in the polymer chain, whereas higher energy states will be spread across a larger portion of the chain. We call these states local ground states (LGSs) and quasi-extended states (QESs), respectively. The classification of states as LGS or QES is performed using the 'signed-value' parameter

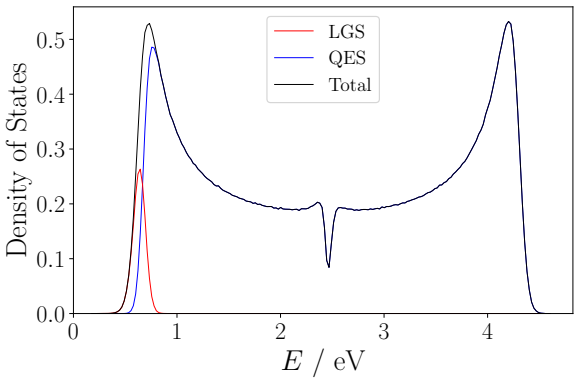

FIG. 3: Density of states in disordered polymer systems, with $\sigma_\epsilon = 0.2$ eV and $\sigma_\phi = 10°$. The distribution of LGSs and QESs is shown individually. LGSs are the energetically lowest lying states.

(SVP)[22]

$$\text{SVP} = \left| \sum_n \psi_n |\psi_n| \right|. \tag{7}$$

where ψ_n is the wavefunction corresponding to the given state, and the sum is taken over all sites, n. ψ_n is found by diagonalizing Eq. (4) for a particular value of the disorder.

We define LGSs as states with a corresponding SVP value greater than 0.95,[22] while the remaining states are classified as QES. The density of states (DOS) shown in Fig. 3 illustrates how the LGSs are the energetically lowest lying states. LGSs lie in the Lifshitz tail of the DOS and have approximately a Gaussian density of states.[30] We note that the dip in the center of the DOS arises because there are two π-conduction (valence) bands, arising from the different LUMO (HOMO) energies of the phenylene and vinylene moieties. The different states and their spatial extents are illustrated in Fig. 4.

Disorder in our model is implemented assuming that both the on-site energies and the torsional angles are assumed to follow a Gaussian distribution, with standard deviations σ_ϵ and σ_ϕ, respectively. Fluctuations in the transfer integral can therefore be quantified by

$$\sigma_t = t_0 \sin(\phi_0)\sigma_\phi. \tag{8}$$

The width of the low energy portion of the density of states is linked to the individual disorder contributions from the on-site energetic and torsional angle fluctuations. The effective disorder contribution from each is given by exchange narrowing[31] as

$$\sigma_{\text{eff}} \sim \frac{\sigma}{\sqrt{L}}, \tag{9}$$

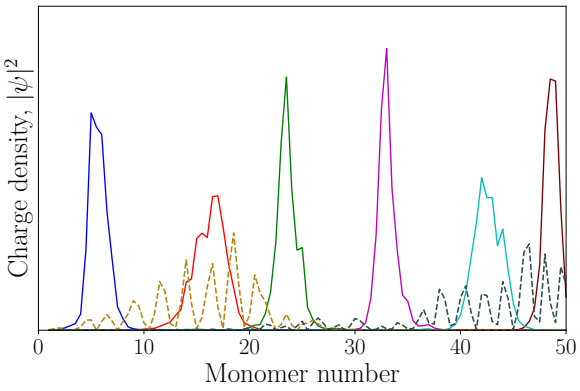

FIG. 4: LGSs (solid lines) and two QESs (dashed lines) for a polymer chain made up of 50 monomer units. LGSs are localized to a few monomer units and are quasi-nodeless, whereas QESs are more delocalized along the chain and have nodes. ψ_n is obtained from Eq. (4).

where L is the localization length. In a system with Gaussian disorder, the localization length near the band edge is lower than at the band center, as has been shown theoretically[22] and numerically,[23,32,33] and is linked to the transfer integral, t, as

$$L \sim \left(\frac{t}{\sigma_t}\right)^{\frac{2}{3}}, \tag{10}$$

and therefore

$$\sigma_{t,\text{eff}} \sim \left(\frac{\sigma_t^4}{t}\right)^{\frac{1}{3}}. \tag{11}$$

For our parameters, shown in Table I, with $\sigma_\phi = 10°$ and $\sigma_\epsilon = 0.2$ eV, we obtain $\sigma_{t,\text{eff}} \sim 8.49$ meV, and $\sigma_{\epsilon,\text{eff}} \sim \sigma_\epsilon/\sqrt{L} \sim 62.5$ meV. Combining these contributions for an overall energetic disorder, we get

$$\sigma_E = \left(\sigma_{\epsilon,\text{eff}}^2 + \sigma_{t,\text{eff}}^2\right)^{\frac{1}{2}} \approx 63\,\text{meV}, \tag{12}$$

which is indeed the FWHM of the LGS portion of the density of states in Fig. 3.

IV. MARCUS THEORY OF TRANSFER RATES

Charge transfer in disordered organic semiconductors is understood to occur via an incoherent hopping mechanism: charge carriers are confined to localized states in the polymer system and evolve in time by hopping between these states, resulting in overall charge transport.[16] This is necessarily a non-adiabatic process by nature.

Hops can occur to nearby localized states (LGSs) and thus charge travels only a short distance with each hop. Alternatively, they can occur to more delocalized states (QESs), ultimately relaxing into a localized state further away. This mechanism was examined in the literature before,[17,18,34,35] and was found to be a relevant competing pathway for diffusion of quasiparticles. Both pathways are therefore implemented in the simulation program.

A. Bimolecular (inter-chain) transfer

Assuming that the normal modes on different polymer chains are decoupled, the inter-chain charge transfer is described by a bimolecular Marcus theory rate expression. In the high-temperature limit ($k_BT \gg \hbar\omega$ for all normal modes considered), when the transfer process is thermally activated, the rate is[36,37]

$$k_{DA,\text{inter}} = \frac{2\pi}{\hbar}|w_{DA}|^2 \int D(E)A(E)\,\mathrm{d}E, \tag{13}$$

where w_{DA} is the resonance transfer integral between donor and acceptor states, and $D(E)$ and $A(E)$ are spectral functions.

The spectral functions for the donor ($X = D$) and acceptor ($X = A$) states are defined as

$$X(E) = \left(\frac{1}{4\pi k_B T E_\lambda}\right)^{\frac{1}{2}} \exp\left(-\frac{(E_X - E_\lambda)^2}{4\pi k_B T E_\lambda}\right), \tag{14}$$

where E_X denotes the energy of the donor and acceptor states

$$E_D = E_{00}^D - E \tag{15}$$

$$E_A = E - E_{00}^A, \tag{16}$$

with E_{00}^X denoting the field-dependent energy of a state, which changes with applied field, $\mathbf{F}$, as a function of the center-of-mass position of the given state, X, as

$$E_{00}^X \to E_{00}^X - q\mathbf{F}\cdot\mathbf{R}^{\text{CoM}}. \tag{17}$$

E_λ is the reorganization energy corresponding to the charge transfer process. The reorganization energy is[38,39]

$$E_\lambda = \hbar\omega \sum_n^{N_{\text{site}}} S_n \left|\psi_n\right|^4 = \hbar\omega S_{\text{eff}}, \tag{18}$$

where S_{eff} is the effective Huang-Rhys parameter and $S_n = A_n^2/2$ takes a value depending to which moiety the site corresponds (see Fig. 1 and Table I for its values). We note that for constant S_n we may express Eq. (18) as

$$E_\lambda = \frac{\hbar\omega S}{\text{PN}}, \tag{19}$$

where PN (the participation number) is $1/\sum_n |\psi_n|^4$ and is proportional to the wavefunction localization length, L. Thus, from Eq. (10) we observe that E_λ is an increasing function of disorder. This observation has implications for the role of disorder on charge mobility, as discussed in Section VI.

For the calculation of the overlap integrals, Mulliken's approximation[40,41] is used, which estimates resonance integrals by the orbital overlap integrals multiplied by a constant. The overlap between the donor and acceptor states, D and A, respectively, is defined as

$$w_{DA} = \sum_n^{N_{\text{site}}} \sum_{i\in n} \sum_m^{N_{\text{site}}} \sum_{j\in m} w_{ij} \left(\varphi_i \psi_n^D\right) \left(\varphi_j \psi_m^A\right), \tag{20}$$

where the orbital overlaps, w_{ij}, between the p-orbitals on atoms i and j, are defined as[40,41]

$$w_{ij} = S_{ij} \times 10.6\,\text{eV}, \tag{21}$$

$$\begin{aligned} S_{ij} = &\cos\Phi_{ij}\, \cos\Omega_{ij}\, \cos\Theta_{ij} \times S_{2p_z,2p_z}(r_{ij}) \\ &- \sin\Omega_{ij}\, \sin\Theta_{ij} \times S_{2p_\sigma,2p_\sigma}(r_{ij}), \end{aligned} \tag{22}$$

with

$$\Phi_{ij} = \arccos\left(\hat{\mathbf{p}}_\mathbf{i} \cdot \hat{\mathbf{p}}_\mathbf{j}\right) \tag{23}$$

$$\Omega_{ij} = \arcsin\left(\hat{\mathbf{p}}_\mathbf{i} \cdot \hat{\mathbf{r}}_\mathbf{ij}\right) \tag{24}$$

$$\Theta_{ij} = -\arcsin\left(\hat{\mathbf{p}}_\mathbf{j} \cdot \hat{\mathbf{r}}_\mathbf{ij}\right), \tag{25}$$

where $\hat{\mathbf{p}}_\mathbf{i}$ and $\hat{\mathbf{p}}_\mathbf{j}$ are the unit vectors parallel to the p_z orbitals on atoms i and j, respectively, and $\hat{\mathbf{r}}_\mathbf{ij}$ is the unit vector parallel to the vector from atom i to j. Finally,

$$S_{2p_z,2p_z}(r) = \exp(-r\xi)\left(1 + r\xi + \frac{2}{5}(r\xi)^2 + \frac{1}{15}(r\xi)^3\right) \tag{26}$$

$$\begin{aligned} S_{2p_\sigma,2p_\sigma}(r) = \exp(-r\xi)\Bigg(&-1 - r\xi - \frac{1}{5}(r\xi)^2 \\ &+ \frac{2}{15}(r\xi)^3 + \frac{1}{15}(r\xi)^4\Bigg), \end{aligned} \tag{27}$$

where $\xi = 3.07\,\text{Å}^{-1}$ and r is the interatomic separation.

B. Unimolecular (intra-chain) transfer

Our model separately allows for charge hopping along a polymer chain. In particular, dynamical torsional fluctuations will cause non-adiabatic transfers via the "fluctuating bridges" mechanism proposed by Skourtis[17] and further examined by Troisi et al.[16,18] This perturbative expression is given by

$$k_{DA,\text{intra}} = k^{(0)} + k^{(2)}, \tag{28}$$

where

$$k^{(0)} = \frac{\langle V^2 \rangle}{\hbar} \sqrt{\frac{\pi}{E_\lambda k_B T}} \exp\left(-\frac{(\Delta E^0 - E_\lambda)^2}{4 E_\lambda k_B T} \right), \tag{29}$$

and

$$k^{(2)} = k^{(0)} \frac{2\hbar^2}{\tau_c^2} \left[\frac{(\Delta E^0 - E_\lambda)^2 - 2 E_\lambda k_B T}{(4 E_\lambda k_B T)^2} \right] \left(1 - \frac{\langle V^2 \rangle}{\langle V \rangle^2} \right). \tag{30}$$

τ_c is the rotational correlation timescale. The second order correction, $k^{(2)}$, is $\sim 1-2$ orders of magnitude smaller than the leading order term. The coupling term, $\langle V^2 \rangle$, arises from torsional rotational motion in the polymer chains and takes the form

$$\langle V_{ij}^2 \rangle = \left(\tilde{t}_0 \sin \phi_0 \right)^2 \left(\frac{k_B T}{K_{\text{tor}}} \right) \sum_{n=1}^{N-1} \left\{ (\psi_n^i \psi_{n+1}^j)^2 + (\psi_n^i \psi_{n-1}^j)^2 \right\}, \tag{31}$$

where $\tilde{t}_0$ is the transfer integral, ϕ_0 is the mean torsional angle between neighboring monomers in the chain, and K_{tor} is the elasticity constant for torsional motion. In Eq. (31) we have used $\langle \delta\phi^2 \rangle = k_B T / K_{\text{tor}}$ from the principle of equipartition.

The reorganization energy for intramolecular transfer is determined by considering the two states involved, D and A, on the polymer chain. Generalising Eq. (18), this is

$$E_\lambda = \hbar\omega \sum_n^{N_{\text{site}}} S_n \left\{ (\psi_n^D)^2 - (\psi_n^A)^2 \right\}^2, \tag{32}$$

where S_n is the Huang-Rhys parameter for the n^{th} moiety as described above.[42]

In principle, dynamical torsional fluctuations also cause an adiabatic time evolution of states, leading to a "crawling" motion along the chain.[43,44] This mechanism is not described in the current work.

TABLE I: Parameters used in the simulations.

Phonon energy	$\hbar\omega$	0.2 eV
Huang-Rhys parameter (phenylene)	S_P	0.91
Huang-Rhys parameter (vinylene)	S_V	2.00
Transfer integral	$\tilde{t}_0$	0.90 eV
Phenylene on-site interaction	ϵ_P	2.4 eV
Vinylene on-site interaction	ϵ_V	2.6 eV
Mean torsional angle	ϕ_0	10°
On-site energetic disorder	σ_ϵ	$0.0 - 0.4$ eV
Torsional disorder	σ_ϕ	$10 - 20°$
Probability of cis/trans defects	$P_{\text{cis/trans}}$	0% or 10%
Elasticity for torsional motion	K_{tor}	10.5 eV
Rotational correlation time	τ_c	15 ps
Average monomer spacing		4 Å

V. MODELING CHARGE TRANSPORT

A. Building polymer conformations

Polymer chain conformations are generated through a series of vector additions, building up the polymer chains by one monomer unit at a time, starting and ending with a phenylene unit. Fixed bond lengths of 1.39 Å, 1.33 Å and 1.44 Å for the phenylene ring, the vinylene double bond and the single linking bond between the moieties, respectively, are used.[45] The bond angles in the phenylene ring, as well as the angle between the single and double bond of the vinylene units, is 120°. The values (both mean and standard deviation) of the torsional angles – assumed to follow a Gaussian distribution – between the planes of the neighboring phenylene and vinylene units are controlled by input parameters of the simulation, as shown in Table I. The average monomer spacing[46] is used to calculate the volume of the simulation box. Generated polymer chains are then randomly distributed within the calculated simulation box. Periodic boundary conditions are implemented with 18 neighboring boxes (side and edge-sharing boxes of the 'home' box). The periodic boundary

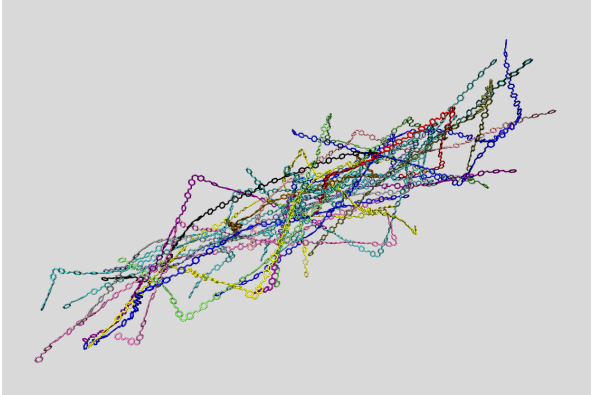

FIG. 5: Randomized polymer chain morphology from the simulation code, showing 'home box' polymer chains only.

conditions mean that when a charge lands in one of the neighboring simulation boxes, it is reset to the equivalent state in the 'home' box before the next charge transfer event. The system size considered in the simulations is 100 polymer chains of 300 ring units (or 599 coarse-grained sites) each, as charge mobilities were found to plateau as a function of size at these values. The option to add cis/trans defects in the vinylene units with a given probability is controlled by the input parameters.

B. Kinetic Monte Carlo simulation

Charge dynamics in the system is simulated by a kinetic Monte Carlo (kMC) scheme in the calculated disordered energetic landscape with hopping transfer between the designated donor-acceptor states. The method implements a directed random walk of charge with variable time steps and variable hopping distances, following closely the method initially proposed by Bässler.[6] Considering a donor state, D, with n potential acceptor states, A_i, the charge carrier hops into a randomly selected acceptor state, selected with a probability:

$$P_{D\to A_i} = \frac{k_{D\to A_i}}{\sum_{i=1}^{n} k_{D\to A_i}}. \tag{33}$$

The charge carrier then spends a certain amount of time (dwells) in this state, selected from the exponential distribution with a mean defined as the reciprocal of the total transition

rate out of this state:

$$\langle t_{\mathrm{dwell},D} \rangle = \frac{1}{\sum_{i=1}^{n} k_{D \to A_i}}, \tag{34}$$

where D now denotes the state the charge carrier landed in, i.e., the previous acceptor state/the new donor state for the next jump. This approach allows for certain states to 'trap' the charge and therefore lower the drift velocity, and consequently the mobility. This formulation of transition rates incorporates a link to the torsional dynamics of chains via the rotational correlation timescale, τ_c. For PPV systems, this is estimated to be $\sim 15\,\mathrm{ps}$.[47] We therefore argue that this is the longest timescale that a charge is allowed to dwell in a state within the framework of the static disorder model; a longer charge trapping time is avoided by randomly placing the charge carrier into a different donor state on the same chain and continuing the random walk of the charge carrier from that state.

The relaxation from QES to LGS states is assumed to be significantly faster than the hops between LGS states and LGS to QES states, and is therefore assumed to occur instantaneously. The probability of this rapid intramolecular relaxation, P_{if}, is defined by

$$P_{if} = \frac{\alpha_{if}}{\sum_{f} \alpha_{if}}, \tag{35}$$

where

$$\alpha_{if} = \sum_{n} |\psi_n^i|^2 |\psi_n^f|^2 \tag{36}$$

and the sums are taken over all sites on the chain, n, and the initial QES state and final LGS state on the same chain are denoted by ψ_n^i and ψ_n^f, respectively. This means that only LGSs can act as donor states in our model.

Each kMC random walk is run until a set total simulation time is achieved; the displacement as a function of time is used to calculate the drift velocity and hence the charge mobility. Sampling over a large number of trajectories and multiple polymer morphologies was performed at each field strength value and initial parameter set to obtain results with no significant statistical fluctuations. In practice, this meant 10 MC trajectories initiated on each polymer chain in the simulation 'home' box (1000 MC trajectories), and the process was repeated over $5-10$ realizations of the randomized structural and energetic landscape, through the use of different random number seeds, leading to $5000-10000$ total MC trajectories at each given set of parameters. Outlier values (MC trajectories resulting in charge

mobilities more than two standard deviations away from the total sample mean) were excluded from the final averages. Each MC trajectory was run for a sufficiently long time that the time dependence of charge displacement, $\langle L(t) \rangle$, was in the linear, i.e., drift-controlled, regime. This is explained in more detail in the Supplementary Information.

Charge mobility values were obtained from averaging the drift velocities obtained from each MC trajectory, and then using the drift mobility formula

$$\mu = \frac{q \langle v(F) \rangle}{F}, \tag{37}$$

where $v(F)$ is the field-dependent drift velocity of the charge carrier and q is its charge.

In the model, various tuneable parameters were used, and are presented in Table I. In particular, for the various values of on-site disorder ($\sigma_\epsilon = 0.0 - 0.1 - 0.2 - 0.4$ eV), the effective disorder, σ_E, i.e. the width of the LGS portion of the total DOS, was found to be $28 - 143$ meV, which is $\sim (1 - 5) \times k_B T$ at 298 K. This is in agreement with values reported elsewhere in the literature.[6,48–50]

VI. RESULTS AND DISCUSSION

A. Mobility with exclusively LGSs hopping mechanism

1. Electric field dependence

Charge mobility was initially examined via hopping between the highly localized, low energy states (LGSs) only. The dependence of average transition rates, hopping distances and ultimately charge mobility on temperature, disorder and polymer chain orientations are presented in this section.

The average rates shown in Fig. 6 are the means of the sums of transition rates, $\langle \sum_A k_{DA} \rangle_D$, out of each possible donor states, D, i.e., the total rate of charge carriers flowing out of a given donor state. A linear $\log k_{DA}$ vs $-\sqrt{F}$ regime is observed at high fields, despite none of the rate expressions used in the model containing this proportionality explicitly. The observation that in the high field regime higher disorder leads to higher transition rates is explained by the facts that first, at low disorder with a narrower DOS, the energetic differences between states are lower and so the large field bias pushes the system

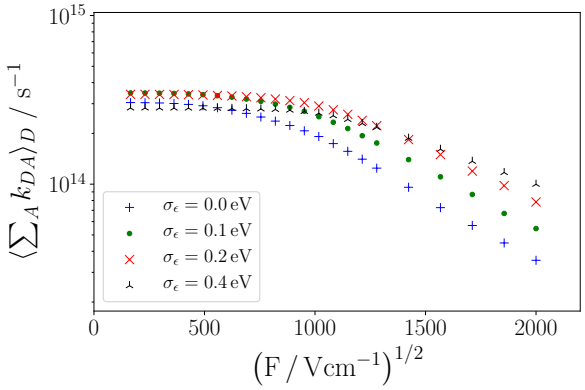

FIG. 6: The total charge carrier escape rates from donor states as a function of electric field, averaged over all possible donor states, plotted at various levels of on-site disorder for randomly oriented chains with 10% cis/trans defects, 10° torsional disorder at 298 K temperature. LGSs to LGSs only transitions.

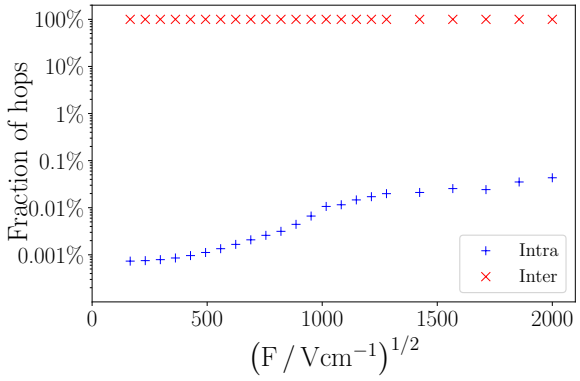

FIG. 7: Fraction of hops being either inter or intramolecular for the kMC. Same simulation parameters as Fig. 6, with $\sigma_\epsilon = 0.2$ eV. LGSs to LGSs only transitions.

further into the Marcus inverted regime than for higher disorder. Second, as Eqs. (10) and (19) show, the Marcus inverted regime occurs at a higher field for higher disorder.

Fig. 7 shows the fraction of hops that took place in the kMC simulations, being classified either as an intermolecular or intramolecular transition. It is observed that charge transport seems to be driven almost exclusively by intermolecular hops, across all field strength values. This is explained by the small spatial overlap between LGSs found on the same polymer chain (as shown in Fig. 4), leading to low intramolecular transition rates.

Charge mobilities were calculated over a range of parameters and field strength values; the results presented in Fig. 8 demonstrate the trends observed in charge mobilities as a

response to changing a single simulation parameter in turn.

Three different relative orientations of polymer chains were considered. A quasi-parallel orientation of the polymer chains was ensured by aligning the end-to-end vectors of polymer chains. For quasi-parallel chains, the simulations were performed both with the electric field parallel (longitudinal) to the common chain orientation as well as it being applied in the perpendicular (transverse) direction. Further to these, a more realistic model of disordered polymer chains, i.e., molecules with randomized alignment was also investigated. The variation in charge mobility with orientation is presented in Fig. 8a, showing that the mobility is independent of chain orientations in the low field regime. At high fields, however, the higher mobilities were observed for transverse and randomly oriented chains, both being significantly higher than the longitudinal case. This can be explained by the low intramolecular transition rates for LGS-only transitions, as it would be mostly intramolecular hops resulting in charge movement along the field direction in the longitudinal case.

In real polymer systems, structural defects in the form of cis/trans defects can be observed, leading to some of the vinylene units taking a cis bond arrangement rather than the energetically favorable trans one, resulting in the coiling of polymer chains. In Fig. 8b it is shown that coiling of the chains results in significantly higher mobilities, as this structural defect can bring intermolecular donor-acceptor pairs closer together spatially, improving wavefunction overlaps and therefore transition rates.

The effect of varying on-site energetic disorder in the polymer chains is shown in Fig. 8c. The effect of disorder is larger at low fields, which can be attributed to the larger disorder resulting in larger activation barriers to charge transfer. The effect of these differences diminishes as the applied energetic bias due to the electric field increases. As with the transition rates presented in Fig. 6, the inversion at high fields was observed once again – increasing disorder leads to slightly, but consistently higher mobilities. The explanation for this is that the higher levels of disorder lead to wider distribution of donor-acceptor energetic differences, as well as the localized states becoming more localized spatially, leading to larger reorganization energies. Both of these contributions have the potential effect of counteracting large energetic biases coming from the applied electric field, leading to higher transition rates, due to being pushed less far into the Marcus inverted regime. This behavior is further examined and confirmed in the Supplementary Information. The same trends emerge from changing the level of structural (torsional) disorder, shown in Fig. 8d.

Figs. 8c and 8d indicate that in the low-field (normal Marcus) regime the role of disorder is significant: doubling either the on-site or torsional disorder leads to a reduction in the mobility by up to two orders of magnitude. Experimentally measured charge mobilities for PPV-based systems range between $10^{-8} - 10^{-3}$ $\mathrm{cm^2\,V^{-1}\,s^{-1}}$ based on the applied field strength value and charge carrier density.[2,48,51–56] This suggests that the larger levels of disorder show better quantitative agreement with experimental results. The effective disorder, σ_E, for $\sigma_\epsilon = 0.2$ eV and $\sigma_\phi = 20°$ is ~ 156 meV, and for $\sigma_\epsilon = 0.4$ eV and $\sigma_\phi = 10°$, it is ~ 143 meV. These values are close to the disorder parameters reported in the literature, obtained from fitting Bässler's formula to experimental measurements.[49] We discuss more realistic modeling for PPV in Section VI C.

2. Temperature dependence

Next, the temperature dependence of charge mobility was examined. As shown in Fig. 8e, changing the simulation temperature was found to only affect mobilities at low fields, as the results converge at high fields, where the energetic differences due to the applied field bias become the dominant driving force. The differences in low fields behavior is interpreted as follows: at 120 K and 180 K the thermal energy is too low to overcome all the activation barriers to transport, and therefore charge mobility is initially increased by the application of a field bias, until a maximum is reached, at which point the reduction due to entering the Marcus inverted regime occurs. As the temperature is increased, the gradient of low field mobility decreases, and becomes slightly negative at 400 K. This change is in qualitative agreement with the generally accepted[6–9] experimentally verified[55,57,58] relation describing charge mobility presented in Eq. (1).

Fishchuk and co-workers developed[11] a unified description of charge mobility at low fields, accounting for both polaron and disorder effects, leading to the temperature dependence described by Eq. (1), namely

$$\mu(T) \propto \exp\left[-\left(\frac{E_a}{k_B T}\right)\right] \exp\left[-C\left(\frac{\sigma}{k_B T}\right)^2\right], \tag{38}$$

where the terms are the same as those described for Eq. (1). In this description, the first term is an Arrhenius-type dependence, capturing polaronic effects, whereas the second term accounts for disorder effects. As shown in Figs. 8c to 8e already, our model produces results

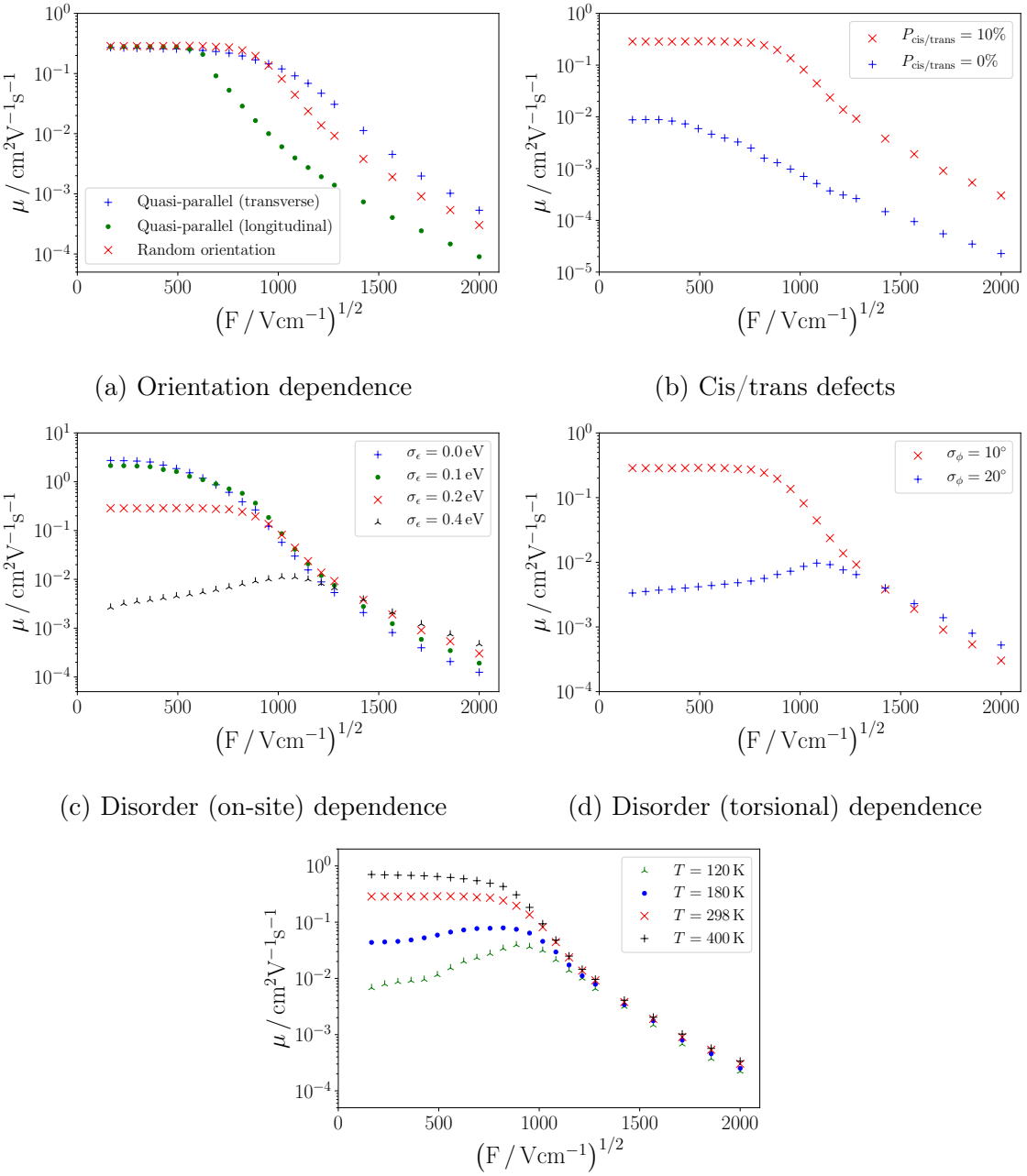

(a) Orientation dependence

(b) Cis/trans defects

(c) Disorder (on-site) dependence

(d) Disorder (torsional) dependence

(e) Temperature dependence

FIG. 8: Charge mobilities obtained from simulations involving hops between low-energy localized grounds states (LGSs) only. Presented are results with varying (a) relative chain and electric field orientations, (b) levels of cis/trans disorder, (c) magnitude of on-site energetic disorder, (d) magnitude of torsional disorder, and (e) temperatures of simulation. The parameter set for the data set in red is the same in all plots, i.e., randomly oriented chains with 10% cis/trans defects, 0.2 eV on-site and 10° torsional disorder at 298 K temperature. The parameters for the other data sets are the same, except as indicated otherwise in the legends.

which are consistent with the second term, showing a reduction in charge mobility both with increased disorder and lower temperatures. Fishchuk's analysis predicts a cross-over between disorder and polaron controlled transport at a critical temperature,

$$T_c = \frac{C}{k_B E_a}\sigma^2, \tag{39}$$

where the factor C depends on the ratio of disorder, σ, and polaron activation energy, E_a, which itself can be obtained in terms of the reorganization energy, E_λ, as $E_a = E_\lambda/4$. Based on our model parameter set, corresponding to $\sigma_E \approx 62.5$ meV and $E_\lambda \approx 19$ meV, this expression predicts $T_c \approx 1000$ K, suggesting disorder controlled transport at all temperatures probed in this work. This prediction was examined through the behavior of mobility, plotted against both $1/T$ and $1/T^2$, as shown in Figs. 9a and 9b. Based on these figures, we cannot conclusively deduce either polaron or disorder dominated transport behavior, but the Arrhenius-type, $\log \mu \sim 1/T$, plot (Fig. 9a) is more linear.

We also note that temperature affects the localization length via the temperature dependence of the torsional disorder. As it is difficult to quantify this dependency in the condensed phase, however, such effects are not considered here.

B. Exploring the role of QESs as potential acceptors

The role of the energetically higher lying, more delocalized QESs in charge transport was examined by considering the effect of their inclusion on the transition rates, nature of transport hops, average hopping distances and charge mobility. The number of allowed QES acceptors for each donor state was determined by a spectral overlap cutoff, only keeping donor-acceptor pairs that have sufficient energetic overlap to result in transition rates high enough to compete with the LGSs to LGSs transitions considered previously.

The transition rates presented in Fig. 10 show no significant changes in overall magnitude or in the trends observed for various levels of on-site disorder and the strength of electric field applied, when compared to LGSs only transitions (shown in Fig. 6). This indicates that any differences observed for the charge mobility results with the inclusion of QESs will not be a result of significantly different transition rates.

As a result of the increased hopping distances – states away from the band edge are less localized,[32] so LGS to QES transitions will generally result in larger charge displacement

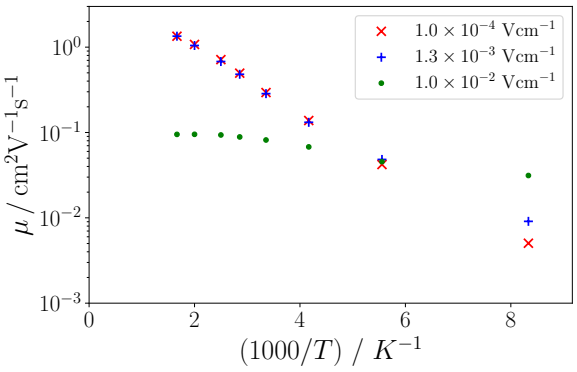

(a)

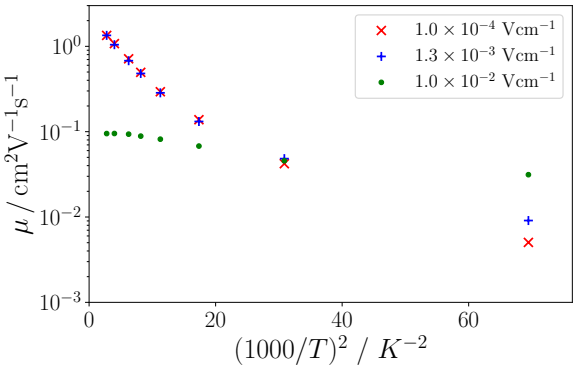

(b)

FIG. 9: Charge mobility, μ, plotted against (a) $1/T$, and (b) $1/T^2$, for temperatures $120 - 600$ K. The lowest field-strength value, shown in red, represents approaching the zero-field limit. The standard parameter set was used, same as in Fig. 8e.

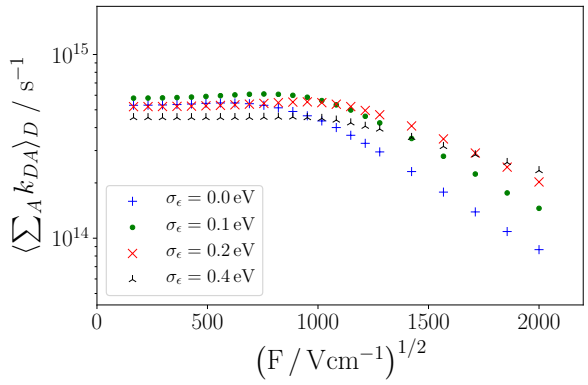

FIG. 10: The total charge carrier escape rates from donor states, averaged over all possible donor states, plotted at various levels of disorder, allowing for LGSs to QESs transitions.

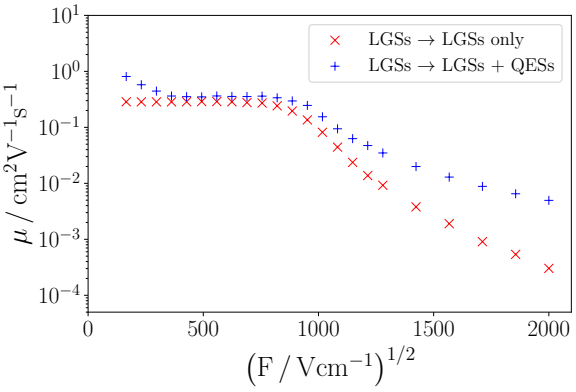

FIG. 11: Comparison of charge mobilities obtained from simulations involving hops between low-energy localized grounds states (LGSs) only as well as from LGSs to QESs. The same parameter set as for the red symbols of Fig. 8.

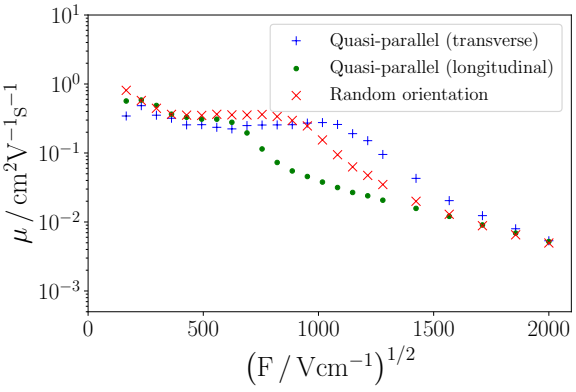

FIG. 12: Field/chain orientation dependence of charge mobility when allowing hops from LGSs to both LGSs and QESs. The inclusion of QESs as acceptor states reduces the system anisotropy. The same parameters as Fig. 8a.

– and the involvement of intramolecular hops in the charge transport process (because of better spatial overlap), charge mobilities are higher at all field strength values when LGS to QES transitions are included. As shown in Fig. 11, it is observed that at very low field values the inclusion of QESs as possible acceptors leads to a small increase in mobility that is difficult to account for, however this feature is also present in simulations and experimental work from Bässler and co-workers.[6,59] Their reasoning for such an increase is that charge carriers may be able to take fast, thermally activated routes partially against the applied electric field, which are shut off as the electric field bias increases. As we do not observe significantly higher transition rates in this field regime, we cannot confirm this reasoning.

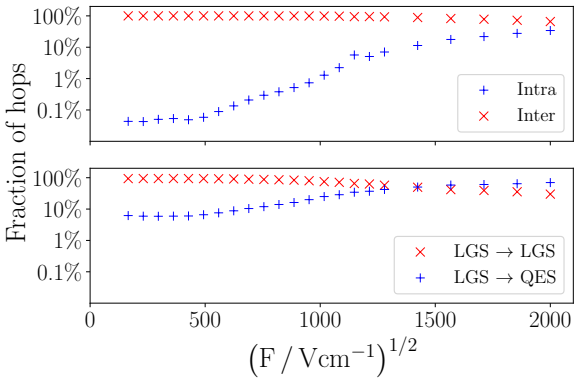

FIG. 13: Fraction of hops occurring either inter or intramolecularly and from either LGS to LGS or LGS to QES, for the same system as in Fig. 7 but with the inclusion of QESs.

We can also discount the possibility of diffusive motion dominating drift motion,[60] because, as shown in the Supplementary Information, the simulation times are always long enough for drift motion to dominate.

For the rest of the low field regime, the differences remain relatively small, but the inclusion of QESs has a significant impact at high fields, leading to an increased mobility by up to two orders of magnitude, while still retaining the decreasing trends in the inverted Marcus regime.

The introduction of QESs as potential acceptors also reduces the dependence of charge mobility on the orientation of polymer chains with respect to each other and the applied electric field, as shown in Fig. 12. At low fields, there is no clearly favored orientation. At mid-field-strength, the same ordering is observed as in Fig. 8a, but at high fields, in the inverted Marcus regime, the mobilities converge again, becoming orientation-independent.

Looking at the hopping ratios in Fig. 13, it is observed that the fraction of intramolecular hops is highly correlated with the fraction of LGS to QES hops. At higher field strength values, intramolecular transport competes equally with intermolecular transport, while LGS to QES transitions become the dominant mode of charge transfer. This is because at higher field strengths the higher energy QESs are pulled down in energy to become quasi-degenerate with the LGSs. This clearly emphasizes the importance of QESs and hence variable range hopping in the intramolecular transport mechanism for large fields.

C. Results from Molecular Dynamics Simulations of Polymer Conformations

Qin and Troisi performed molecular dynamics (MD) simulations on poly(2-methoxy-5-(2'-ethylhexyloxy)-p-phenylene vinylene) (MEH-PPV) oligomer systems.[33] Their simulations on 20 and 40 chains, of 16 monomer units each, were equilibrated at 300 K and dynamics were simulated for 200 ns. Snapshots taken at 0.1 ns intervals were used to obtain structural parameters from their results, leading to dynamics-based parameters for the mean torsional angle, $\phi_0 = 26.6°$, its standard deviation, $\sigma_\phi = 16.8°$, the ratio of cis/trans defects in the vinylene units, $P_{\text{cis/trans}} = 22\%$, and the system density determined monomer spacing, equal to 6 Å. Given that the standard deviation of the transfer integral, σ_t, depends on both the mean and the standard deviation of the torsional angles, as shown in Eq. (8), these represent a higher level of disorder than those previously used in our simulations, and even without on-site energetic disorder, lead to an effective disorder of $\sigma_E = 190$ meV. The equilibrated geometries also confirmed that chains are randomly oriented with respect to each other, in agreement with the orientation previously used as most realistic. Simulations in our model were performed using LGSs to LGSs only transfer using these parameters. As no value of on-site energetic disorder, σ_ϵ, could be extracted from the MD results, this was ignored for the purpose of these simulations to avoid introducing further parametric assumptions not derived from the MD simulations. The charge mobility results are shown in Fig. 14. The trends observed are in agreement with other high disorder simulations, previously presented in Figs. 8c and 8d: low field mobility is field-assisted before reaching a maximum, and then decreases with increasing electric field due to the Marcus inverted regime. This realistic parameter set also reduced the charge mobility in general, leading to a better agreement with experimental values.[2,48,51–56]

VII. SUMMARY AND CONCLUDING REMARKS

We have presented a realistic theory and described the modeling of charge mobility in conjugated polymer thin films. Using realistic conformations of disordered PPV polymer chains, a clear link between polymer structure and the off-diagonal disorder is established. Modeling the competing intra- and intermolecular charge transport processes via Marcus theory allowed an examination of the relative importance of these in bulk charge mobility

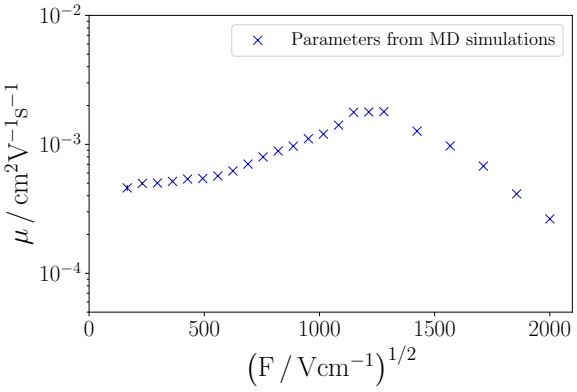

FIG. 14: Charge mobility from simulations with structural parameters obtained from Qin and Troisi's MD simulation.[33]

and the relative roles of localized (LGSs) and quasi-extended (QESs) states. We summarize our findings as follows:

- Our model agrees with experimental observations regarding the electric field dependence of charge mobility at lower field strength values,[57,58] namely that the charge mobility obeys a Poole-Frenkel type, $\log \mu \propto \sqrt{F}$, relation. The gradient of this proportionality changes depending on the relative magnitudes of the effective disorder, σ_E, and thermal energy, $k_B T$, as Eq. (1) would suggest. For higher levels of disorder/lower temperature, the charge mobility is weakly field assisted; for $\sigma_E / k_B T \approx 1$, it is field-independent; and the gradient becomes negative for low disorder/high temperature (see Figs. 8c to 8e). The increasing charge mobility with field strength is a feature that appears in most numerical work based on lattice GDMs and Miller-Abrahams-type rate theory.[6–9] This feature arises in some, but not all experimental charge mobility measurements.[55,57–59,61] Using a realistic theory of donor and acceptor states, our model justifies the predictions of GDMs.

- Examining the temperature dependence of the charge mobility in the framework of Fishchuk and co-workers'[11] description of polaron or disorder controlled transport, we observe a better linear fit for the $\log \mu \sim 1/T$ plot, suggesting polaron controlled transport, but as highlighted by Fishchuk, differentiating a goodness of fit between $\log \mu \sim 1/T$ and $\log \mu \sim 1/T^2$ plots over a limited temperature range is often quite challenging. We therefore cannot conclusively deduce either polaron or disorder controlled transport by our results.

- Our model predicts that the charge mobility undergoes a $\log \mu \propto -\sqrt{F}$ reduction in the high electric field regime, which is observed in the charge transfer rates as well, and is attributed to the high field bias pushing the system into the inverted Marcus regime. This agrees with experimental observations for doped polycarbonate systems[14,62] and analytical work performed in the framework of Marcus theory for 1D systems.[15] Similar conclusions about the high field behavior were reached by numerical work in the framework of Marcus theory.[21]

- We find that including only the highly localized states, LGSs, in the charge transport process leads to an almost exclusively intermolecular transfer mechanism, regardless of disorder, temperature or field orientation. These results are easily rationalized by the poor wavefunction overlap between LGSs on the same polymer chain.

- The inclusion of QESs as potential acceptor states seems particularly important for intramolecular transport, as these states have better spatial wavefunction overlap with LGSs on the same polymer chain. They also enable larger hopping distances with respect to the electric field bias. Thus, there is an increased fraction of intramolecular transport and higher overall charge mobility. The role of higher energy QESs as potential acceptors for donor LGSs becomes especially significant at higher fields, because their energies are pulled down by the electric field. This has consequences for our next conclusion.

- At low and high field strengths the charge mobility is isotropic (i.e., independent of field orientation with respect to molecular orientations). However, at intermediate field values (i.e., $F \sim 5 \times 10^5 - 2 \times 10^6$ V cm^{-1}) the mobility is anisotropic, with larger mobilities in the transverse direction to the average polymer orientation (see Fig. 12). We attribute this behavior to predominantly LGSs to LGSs and hence inter-chain transitions at low fields, while LGSs to QESs and hence intra-chain transitions compete at higher fields (see Fig. 13). This prediction is a potentially key experimental obvservable that distinguishes our model from simpler lattice models.

- The role of disorder is subtle. At low fields (i.e., in the normal Marcus regime), increasing disorder significantly decreases the mobility, because (i) the variation in activation energies is larger than the driving force and (ii) the localization lengths and

hence hopping distances are shorter. However, at higher fields (i.e., in the inverted Marcus regime), increasing disorder slightly increases the mobility, because (i) the increase in reorganization energy (because of the decrease in localization length) with disorder pushes the inverted Marcus regime to higher fields and (ii) increased disorder broadens the density of states (see Figs. 8c and 8d).

- Using structural parameters derived from MD simulations[33] in our model leads to charge mobility values that are in quantitative agreement with experimental measurements. Our model therefore agrees with experimental observations with no adjustable parameters (see Fig. 14).

Our model could be further improved in a number of ways. First, in the current model, quasi-extended states are assumed to relax effectively instantaneously into localized states. According to Mannouch and Barford,[63] however, exciton relaxation in PPV systems is fast, but not instantaneous. Similar treatment of QESs to LGSs relaxation in the framework of time-evolving block decimation (TEBD) could provide a better understanding of the time scale and nature of the charge relaxation process, as well as identifying potential QESs to QESs transitions. The dramatic changes observed in intramolecular transport behavior with and without the more delocalized QESs make understanding this process a priority for us.

Second, the intramolecular transfer process could be more accurately modeled through studying single polymer chains, examining charge motion along the chain as a consequence of Brownian fluctuations in the torsional motion of the chains. As discussed in Section IV B, this causes adiabatic "crawling" motion along the chain. This would also be performed in the framework of TEBD, similar to the work of refs 43 and 44.

SUPPLEMENTARY MATERIAL

See supplementary material for a discussion of the drift and diffusion dominated regimes of charge transport; and a discussion of the role of reorganization energy in controlling the Marcus transport regimes.

ACKNOWLEDGMENTS

We thank Prof. Dr. Heinz Bässler for insightful comments and suggestions on an earlier manuscript. LB is supported by the EPSRC Centre for Doctoral Training, Theory and Modelling in Chemical Sciences (EP/L015722/1). We are also grateful to the UK Materials and Molecular Modelling Hub for computational resources, which is partially funded by EPSRC (EP/P020194/1).

REFERENCES

[1]J. H. Burroughes, D. D. C. Bradley, A. R. Brown, R. N. Marks, K. Mackay, R. H. Friend, P. L. Burns, and A. B. Holmes, Nature **347**, 539 (1990).

[2]K. Pichler, C. P. Jarrett, R. H. Friend, B. Ratier, and A. Moliton, J. Appl. Phys. **77**, 3523 (1995).

[3]Y.-J. Cheng, S.-H. Yang, and C.-S. Hsu, Chem. Rev. **109**, 5868 (2009).

[4]V. Coropceanu, J. Cornil, D. A. da Silva Filho, Y. Olivier, R. Silbey, and J.-L. Brédas, Chem. Rev. **107**, 926 (2007).

[5]M. Jakobsson and S. Stafström, J. Chem. Phys. **135**, 134902 (2011).

[6]H. Bässler, Phys. status solidi **175**, 15 (1993).

[7]Y. Gartstein and E. M. Conwell, Chem. Phys. Lett. **245**, 351 (1995).

[8]D. H. Dunlap, P. E. Parris, and V. M. Kenkre, Phys. Rev. Lett. **77**, 542 (1996).

[9]S. V. Novikov, D. H. Dunlap, V. M. Kenkre, P. E. Parris, and A. V. Vannikov, Phys. Rev. Lett. **81**, 4472 (1998).

[10]P. E. Parris, V. M. Kenkre, and D. H. Dunlap, Phys. Rev. Lett. **87**, 126601 (2001).

[11]I. I. Fishchuk, A. Kadashchuk, S. T. Hoffmann, S. Athanasopoulos, J. Genoe, H. Bässler, and A. Köhler, Phys. Rev. B **88**, 125202 (2013).

[12]W. D. Gill, J. Appl. Phys. **43**, 5033 (1972).

[13]R. A. Marcus, J. Chem. Phys. **24**, 966 (1956).

[14]M. der Auweraer, F. C. De Schryver, P. M. Borsenberger, and H. Bässler, Adv. Mater. **6**, 199 (1994).

[15]K. Seki and M. Tachiya, Phys. Rev. B **65**, 14305 (2001).

[16]R. P. Fornari and A. Troisi, Phys. Chem. Chem. Phys. **16**, 9997 (2014).

[17]S. S. Skourtis, Chem. Phys. Lett. **372**, 224 (2003).

[18]A. Troisi, A. Nitzan, and M. A. Ratner, J. Chem. Phys. **119**, 5782 (2003).

[19]F. C. Grozema and L. D. A. Siebbeles, J. Phys. Chem. Lett. **2**, 2951 (2011).

[20]M. Jakobsson, M. Linares, and S. Stafström, J. Chem. Phys. **137**, 114901 (2012).

[21]N. Lu, L. Li, W. Banerjee, P. Sun, N. Gao, and M. Liu, J. Appl. Phys. **118**, 45701 (2015).

[22]A. V. Malyshev and V. A. Malyshev, Phys. Rev. B **63**, 195111 (2001).

[23]D. V. Makhov and W. Barford, Phys. Rev. B **81**, 165201 (2010).

[24]T. Holstein, Ann. Phys. (N. Y). **8**, 325 (1959).

[25]T. Holstein, Ann. Phys. (N. Y). **8**, 343 (1959).

[26]W. Barford, *Electronic and Optical Properties of Conjugated Polymers (The International Series of Monographs on Physics)* (Oxford University Press, 2005).

[27]O. R. Tozer and W. Barford, Phys. Rev. B **89**, 155434 (2014).

[28]W. Barford, M. Marcus, and O. R. Tozer, J. Phys. Chem. A **120**, 615 (2016).

[29]P. W. Anderson, Phys. Rev. **109**, 1492 (1958).

[30]J. L. Cardy, J. Phys. C Solid State Phys. **11**, L321 (1978).

[31]E. W. Knapp, Chem. Phys. **85**, 73 (1984).

[32]W. Barford and D. Trembath, Phys. Rev. B **80**, 165418 (2009).

[33]T. Qin and A. Troisi, J. Am. Chem. Soc. **135**, 11247 (2013).

[34]A. V. Malyshev, V. A. Malyshev, and F. Domínguez-Adame, J. Phys. Chem. B **107**, 4418 (2003).

[35]A. V. Malyshev, V. A. Malyshev, and F. Domínguez-Adame, Chem. Phys. Lett. **371**, 417 (2003).

[36]V. May and O. Kühn, *Charge and Energy Transfer Dynamics in Molecular Systems* (Wiley-VCH, 2011).

[37]W. Barford, *Electronic and Optical Properties of Conjugated Polymers*, 1st ed. (Oxford University Press, 2009).

[38]W. Barford and M. Marcus, J. Chem. Phys. **141**, 164101 (2014).

[39]M. Marcus, O. R. Tozer, and W. Barford, J. Chem. Phys. **141**, 164102 (2014).

[40]R. S. Mulliken, C. A. Rieke, D. Orloff, and H. Orloff, J. Chem. Phys. **17**, 1248 (1949).

[41]M. Hultell and S. Stafström, Phys. Rev. B **75**, 104304 (2007).

[42]The cross-terms in Eq. (32), i.e., $-2(\psi_n^D)^2(\psi_n^A)^2$ arise because the reorganization energy vanishes when the donor and acceptor states spatially overlap.

[43]N. M. Albu and D. J. Yaron, J. Phys. Chem. C **117**, 12299 (2013).

[44]J. E. Poole, D. A. Damry, O. R. Tozer, and W. Barford, Phys. Chem. Chem. Phys. **18**, 2574 (2016).

[45]P. da Costa, R. G. Dandrea, and E. M. Conwell, Phys. Rev. B **47**, 1800 (1993).

[46]D. R. Gagnon, J. D. Capistran, F. E. Karasz, and R. W. Lenz, Polym. Bull. **12**, 293 (1984).

[47]C. De Leener, E. Hennebicq, J.-C. Sancho-Garcia, and D. Beljonne, J. Phys. Chem. B **113**, 1311 (2009).

[48]M. Gailberger and H. Bässler, Phys. Rev. B **44**, 8643 (1991).

[49]H. C. F. Martens, P. W. M. Blom, and H. F. M. Schoo, Phys. Rev. B **61**, 7489 (2000).

[50]S. M. Gali, G. D'Avino, P. Aurel, G. Han, Y. Yi, T. A. Papadopoulos, V. Coropceanu, J.-L. Brédas, G. Hadziioannou, C. Zannoni, and L. Muccioli, J. Chem. Phys. **147**, 134904 (2017).

[51]A. Kryukov, A. Saidov, and A. V. Vannikov, Thin Solid Films **209**, 84 (1992).

[52]H. Meyer, D. Haarer, H. Naarmann, and H. H. Hörhold, Phys. Rev. B **52**, 2587 (1995).

[53]P. W. M. Blom, M. J. M. de Jong, and J. J. M. Vleggaar, Appl. Phys. Lett. **68**, 3308 (1996).

[54]E. Lebedev, T. Dittrich, V. Petrova-Koch, S. Karg, and W. Brütting, Appl. Phys. Lett. **71**, 2686 (1997).

[55]D. Hertel, H. Bässler, U. Scherf, and H. H. Hörhold, J. Chem. Phys. **110**, 9214 (1999).

[56]C. Tanase, E. J. Meijer, P. W. M. Blom, and D. M. de Leeuw, Phys. Rev. Lett. **91**, 216601 (2003).

[57]A. J. Mozer and N. S. Sariciftci, Chem. Phys. Lett. **389**, 438 (2004).

[58]H. H. Fong, A. Papadimitratos, and G. G. Malliaras, Appl. Phys. Lett. **89**, 172116 (2006).

[59]P. M. Borsenberger, L. Pautmeier, and H. Bässler, J. Chem. Phys. **94**, 5447 (1991).

[60]S. D. Baranovskii, Phys. status solidi **251**, 487 (2014).

[61]L. B. Schein, A. Peled, and D. Glatz, J. Appl. Phys. **66**, 686 (1989).

[62]M. Novo, M. van der Auweraer, F. C. de Schryver, P. Borsenberger, and H. Bässler, Phys. status solidi **177**, 223 (1993).

[63]J. R. Mannouch, W. Barford, and S. Al-Assam, J. Chem. Phys. **148**, 34901 (2018).